

Double Occupancy and Magnetic Susceptibility of the Anderson Impurity Model out of Equilibrium

A. DIRKS^{1,2,3}, S. SCHMITT^{4 (a)}, J.E. HAN², F. ANDERS⁴, P. WERNER⁵ and T. PRUSCHKE¹

¹ *Institut für Theoretische Physik, Universität Göttingen, D-37077 Göttingen, Germany*

² *Department of Physics, State University of New York at Buffalo, Buffalo, NY 14260, USA*

³ *Department of Physics, Georgetown University, Washington, DC 20057, USA*

⁴ *Lehrstuhl für Theoretische Physik II, Technische Universität Dortmund, D-44221 Dortmund, Germany*

⁵ *Department of Physics, University of Fribourg, CH-1700 Fribourg, Switzerland*

PACS 72.15.Qm – Scattering mechanisms and Kondo effect

PACS 73.63.Kv – Electronic transport in nanoscale materials and structures: Quantum dots

Abstract – We use different numerical approaches to calculate the double occupancy and magnetic susceptibility as a function of a bias voltage in an Anderson impurity model. Specifically, we compare results from the Matsubara-voltage quantum Monte-Carlo approach (MV-QMC), the scattering-states numerical renormalization group (SNRG), and real-time quantum Monte-Carlo (RT-QMC), covering Coulomb repulsions ranging from the weak-coupling well into the strong-coupling regime. We observe a distinctly different behavior of the double occupancy and the magnetic response. The former measures charge fluctuations and thus only indirectly exhibits the Kondo scale, while the latter exhibits structures on the scale of the equilibrium Kondo temperature. The Matsubara-voltage approach and the scattering-states numerical renormalization group yield consistent values for the magnetic susceptibility in the Kondo limit. On the other hand, all three numerical methods produce different results for the behavior of charge fluctuations in strongly interacting dots out of equilibrium.

Introduction. – The advances in nanostructuring of heterogeneous semiconductors and in the handling of molecules have made it possible to reproducibly build carefully designed nanometer-scale devices. These generically consist of a few locally interacting degrees of freedom, for example in a quantum dot in contact with macroscopic leads. The spatial confinement of the quantum dot electrons to a few nanometers implies a small electrical capacitance C and, hence, a sizable charging energy $U = e^2/C$. The attraction of such devices stems from their highly controllable properties [1,2]. Substantially increasing the coupling to the leads but still maintaining the charge fluctuation scale below charging energy tunes the quantum dots into the experimentally accessible Kondo regime [3–6]. This regime is characterized by the lifting of the Coulomb blockade [1] in the quantum transport at temperatures below a dynamically generated small energy scale, called Kondo temperature T_K , which ubiquitously shows up in physical properties [7].

The experiments performed on mesoscopic systems typically are measurements of transport properties in the presence of external fields and voltage bias, making a theoretical description in terms of non-equilibrium statistical physics mandatory. The theoretical challenge of the Kondo regime is related to the change of ground state [7] upon cooling the system from an intermediate-temperature local-moment regime to the low-temperature regime which manifests itself in the lifting of the Coulomb blockade at zero bias. This crossover cannot be reliably accessed by any finite order perturbation theory in the Coulomb repulsion and requires more sophisticated analytical methods such as Bethe ansatz [8] or numerical methods such as Wilsons numerical renormalization group (NRG) [9].

However, no exact solution for the transport properties through quantum dots at finite bias exists for models of interacting quantum many-body systems out of equilibrium. Over the past two decades, several approaches have been developed to approximately or numerically solve such models, ranging from perturbation theory [10–12]

^(a)Present address: Honda Research Institute GmbH, D-63073 Offenbach, Germany

and renormalization approaches [13–15] to various numerical techniques [16–22]. Most of these approaches work well in certain limits, where Kondo physics is either not yet relevant or – due to strong external fields – already suppressed. Accessing the crossover regime where external fields, in particular the bias voltage across the dot, are of the order of the Kondo temperature, remains a great challenge.

In this paper we present results for static quantities of a quantum dot in steady-state non equilibrium for dot parameters, temperatures, and voltages that fall precisely into this challenging regime. One approach employed here has been recently proposed by Han and Heary [23]. It maps the steady-state non-equilibrium system onto an infinite set of auxiliary equilibrium statistical-physics problems. The latter are solved by a continuous-time quantum Monte-Carlo algorithm [24, 25]. The main challenge in this approach is to map the auxiliary systems back onto the real one, which can be accomplished by a standard maximum entropy analytical continuation procedure [26]. Details of the numerical procedure have been provided in a recent publication [27]. Here, we compare the results of this Matsubara-voltage quantum Monte Carlo (MV-QMC) approach to data obtained with a scattering-states numerical renormalization group (SNRG) method [19, 29, 30] and real-time quantum Monte Carlo (RT-QMC) [17, 18].

Model and Methods. – The simplest and most frequently used model for a quantum dot is the single-impurity Anderson model [4]. In this model, the dot is described by a single molecular orbital, which can accommodate up to two electrons. In the doubly occupied case the Coulomb repulsion leads to a charging energy of U . The dot orbital is connected via single-particle tunneling of amplitude t_α to two continuous sets of non-interacting fermionic baths, which are called *source* and *drain lead*, and are indicated by an index $\alpha = \pm 1$. The leads can have different chemical potentials, and the difference $e\Phi = \mu_{-1} - \mu_{+1}$ in chemical potentials represents the physical *bias voltage*. With these conventions, the Hamiltonian reads

$$H = \sum_{\alpha k \sigma} \epsilon_{\alpha k \sigma} c_{\alpha k}^\dagger c_{\alpha k \sigma} + \sum_{\sigma = \pm 1} (\epsilon_d + \sigma B) d_\sigma^\dagger d_\sigma + U n_{d, \uparrow} n_{d, \downarrow} + \sum_{\alpha k \sigma} \left(\frac{t_\alpha}{\sqrt{\Omega}} c_{\alpha k \sigma}^\dagger d_\sigma + \text{h.c.} \right), \quad (1)$$

where $c_{\alpha k \sigma}^\dagger$ and d_σ^\dagger are the usual fermionic creation operators of electrons with spin $\sigma = \{\pm 1\} = \{\uparrow, \downarrow\}$, in lead $\alpha = \pm 1$ with momentum k or on the dot ($\hbar = c = k_B = 1$). The corresponding single-particle energies are $\epsilon_{\alpha k \sigma}$ and ϵ_d , respectively, and we added the Zeeman energy $\sigma B = \sigma g \mu_B H / 2$ into the single-particle energy on the dot, which includes the effect of an external magnetic field H . We will consider the wide-band limit for the leads with symmetric coupling $t_- = t_+ = t$ and the particle-hole symmetric

point $\epsilon_d = -U/2$. Ω denotes the phase space volume. As unit of energy we use the Anderson width $\Gamma = 2\pi t^2 \mathcal{N}_F$, where \mathcal{N}_F is the conduction electron density of states at the Fermi energy.

The method developed by Han and Heary employs a complexification of the physical bias voltage $\Phi \rightarrow i\varphi_m$ with $\varphi_m = 4\pi m / \beta$ (Matsubara voltages) [23], which results in an infinite set of auxiliary equilibrium statistical-mechanics systems one can efficiently solve by state-of-the-art Monte Carlo algorithms [24, 25]. The mapping back to non-equilibrium quantities is done via analytical continuation $i\varphi_m \rightarrow \Phi \pm i\delta$ from the Matsubara voltages to the real voltage. A central goal is of course the calculation of transport properties. Unfortunately, the non-locality of the current operator and the rather complicated analytical structure of the local Green’s functions render such calculations very difficult [28]. However, obtaining results for static local quantities, such as the double occupancy on the dot or the magnetization, is relatively straightforward [27].

The full derivation of the formulas connecting those static quantities in the Matsubara voltage space with the real-voltage expectation value were presented in Ref. [27]. For local observables \mathcal{O} , such as the double occupancy and magnetization of the dot, one finds the representation

$$\langle \mathcal{O} \rangle (i\varphi_m) = \langle \mathcal{O} \rangle |_{\varphi_m \rightarrow \infty} + \int \frac{\varrho_{\mathcal{O}}(\varphi)}{(i\varphi_m - \Phi) - \varphi} d\varphi, \quad (2)$$

with $\varrho_{\mathcal{O}}(\varphi)$ the spectral function. The physical expectation value is then given by [27]

$$\langle \mathcal{O} \rangle_{\text{neq}} = \langle \mathcal{O} \rangle |_{\varphi_m \rightarrow \infty} - \mathcal{P} \int \frac{\varrho_{\mathcal{O}}(\varphi)}{\varphi} d\varphi, \quad (3)$$

where $\mathcal{P} \int \dots$ denotes the principal value integral.

Highly precise data for $\langle \mathcal{O} \rangle (i\varphi_m)$ can be obtained even for large values of φ_m from the effective equilibrium systems of the Matsubara voltage representation by use of the continuous-time quantum Monte Carlo (CT-QMC) technique [25]. In contrast to equilibrium QMC for the Anderson impurity model, we expect a sign- respectively phase-problem here due to the presence of a complex quantity in the effective action. It turns out, however, that this phase problem is rather weak for small to intermediate bias, although it can become significant for large bias voltage and very large $i\varphi_m$.¹

The representation (2) is formally similar to the standard Lehmann-type representation of correlation functions. Due to the singular nature of the integral equation (2), the numerical determination of the spectral function $\varrho_{\mathcal{O}}(\varphi)$ from QMC data is known to be an ill-posed problem. An adequate tool which helps to reduce uncontrollable biases in the estimates of $\varrho_{\mathcal{O}}(\varphi)$ is provided by the maximum entropy method (MaxEnt) [26]. It uses

¹For example, for $i\varphi_m = 60$ we find for certain model parameters ($U = 8\Gamma$, $\beta\Gamma = 20.0$, $B = 0.04\Gamma$) average phase factors $|\langle e^{i\gamma} \rangle| \approx 0.073$ at $e\Phi = 2\Gamma$, and $|\langle e^{i\gamma} \rangle| \approx 0.40$ at $e\Phi = 1\Gamma$.

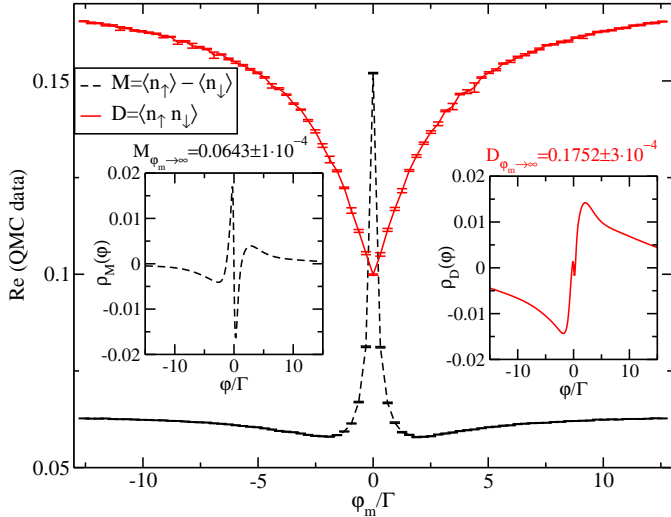


Fig. 1: Raw data used in the computation of the magnetization M and double occupancy D of a quantum dot ($U = 8\Gamma$, $\beta\Gamma = 40$, $B = 0.02$, $e\Phi = 0.01\Gamma$) in MV-QMC. The insets show the inferred offsets and spectral functions which yield the physical value.

Bayesian inference by interpreting the spectral function as a probability density. A-priori and a-posteriori information about this density and quantities derived from it can be discriminated and discussed properly. As an illustration of the procedure, we plot in Fig. 1 the raw data for the calculation of the magnetization M and double occupancy D in a model with $U = 8\Gamma$, $\beta\Gamma = 40$, $B = 0.02\Gamma$, $e\Phi = 0.01\Gamma$. The offsets inferred from these QMC results are $M_{i\varphi_n \rightarrow \infty} = 0.0643(1)$ and $D_{i\varphi_n \rightarrow \infty} = 0.1752(3)$ and the spectral functions obtained from the MaxEnt procedure are shown as insets. With these results, Eq. (3) leads to $M = 0.134(1)$ and $D = 0.107(9)$.

In order to analyze the numerical results of the Matsubara-voltage technique in the strongly correlated regime quantitatively, we compare them to SNRG [19, 29, 30] and real RT-QMC [17, 18] calculations.

The SNRG method extends the well-known equilibrium numerical renormalization group (NRG) [9] to describe steady-state non-equilibrium transport through interacting nano-devices. The method starts from a formulation of the noninteracting $U = 0$ problem in terms of exactly known scattering states, which are the solutions of the Lippmann-Schwinger equations [29]. Therefore, the boundary conditions of the open quantum system with particles entering and leaving the whole system are correctly incorporated. Formulating the NRG in the basis of these scattering states allows for the application of the time-dependent NRG [31, 32]. Starting from the initial $U = 0$ Hamiltonian the interaction U is switched on and the time-evolution of the system is calculated. The results for the long-time steady state limit can be accessed analytically and steady-state nonequilibrium expectation values are calculated for arbitrary interaction strength and

bias voltage.

The RT-QMC technique [17, 18] is used to check the non-equilibrium double occupancies. This method computes steady-state expectation values by performing a quench, either in the interaction U or the voltage bias Φ , and is based on a stochastic sampling of weak-coupling diagrams within the Keldysh real-time Green's function approach. The technique employed here is the interaction quench, described in detail in Ref. [18]. We start from the noninteracting system with applied bias voltage and switch on the interaction at time $t = 0$. The time-evolution of the double occupancy is then computed by randomly placing interaction vertices on the Keldysh contour, using a Monte Carlo technique. As a result of the quench, the double occupancy decreases and eventually approaches a time-independent value corresponding to the steady-state double occupancy of the interacting system [17]. If the times accessible in the RT-QMC calculation are long enough to see this convergence, the results are numerically exact. Difficulties arise in the small-voltage regime, where the transient dynamics becomes slow (the longest accessible time is limited by a dynamical sign problem in the Monte Carlo sampling). The double occupancy is easier to measure than the magnetic susceptibility, because in a half-filled dot with symmetric bias, only even perturbation orders contribute to the observable, which reduces the dynamical sign problem.

Results. –

Double occupancy. The double occupancy $D = \langle n_\uparrow n_\downarrow \rangle$ is usually not discussed in the context of Kondo physics, and therefore we believe it is useful to start here with a study of the equilibrium behavior of this quantity in the absence of an external magnetic field, $B = 0$. We consider the particle-hole symmetric case where $\langle n_d \rangle = \langle n_\uparrow + n_\downarrow \rangle = 1$, and the double occupancy measures the charge fluctuation of the quantum dot, i.e.

$$D = \langle n_\uparrow n_\downarrow \rangle = \frac{1}{2} \langle (n_d - 1)^2 \rangle = \frac{1}{2} \langle (n_d - \langle n_d \rangle)^2 \rangle. \quad (4)$$

This quantity is shown as a function of T in Fig. 2 for various values of the Coulomb repulsion U . The high temperature limit $D(T \gg \Gamma, U) \approx \langle n_\uparrow \rangle \langle n_\downarrow \rangle = 1/4$ is approached by all curves (not explicitly shown), and the low temperature saturation values roughly scale as $1/U$, as expected (see lower right inset of Fig. 2(a)). However, the first striking observation is that, in contrast to e.g. the magnetization, one does not see any explicit signature of the Kondo scale. Instead, for all values of U a minimum appears for temperatures on the scale of $T \approx \Gamma$ with weakly temperature dependent tails at lower T . The information about T_K is contained in these tails. Plotting $F(T) := 1 - D(T)/D(T=0)$ as a function of T/T_K (main panel of Fig. 2(a)) we find a nice scaling for $T \lesssim T_K$. The curves for all U fall on top of each other and follow a quadratic behavior, $F(T \rightarrow 0) \sim (T/T_K)^2$, which is consistent with the Fermi liquid nature of the strong-coupling

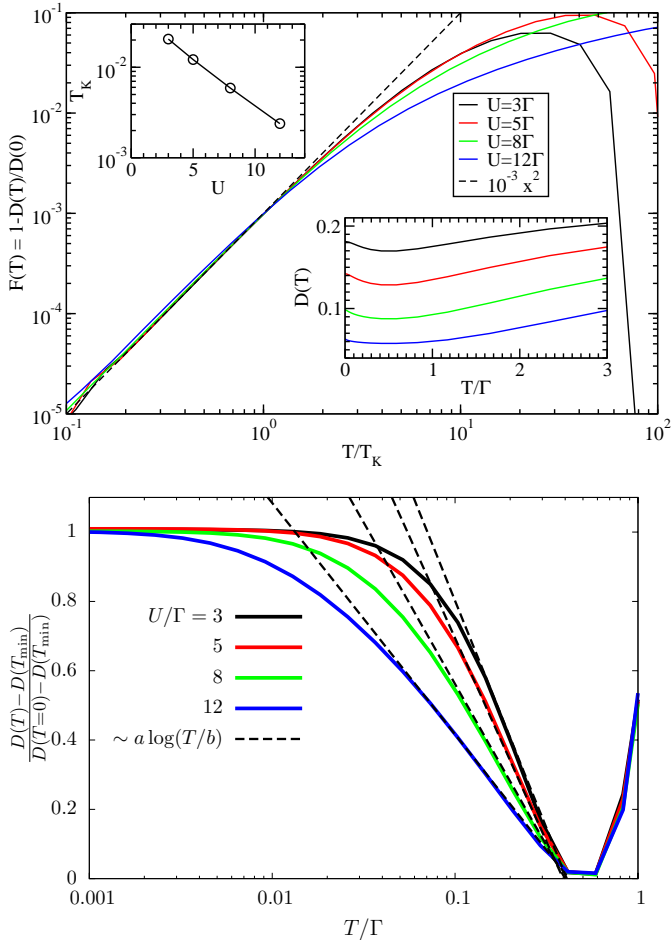


Fig. 2: Equilibrium NRG results. (a) The scaling function F of the double occupancy D as a function of temperature in units of the Kondo temperature for various values of U . The dashed line shows the quadratic function $0.001x^2$. The lower right inset shows the double occupancy $D(T)$ as a function of temperature in units of Γ . The upper left inset shows the Kondo scale as extracted from a fit to the scaling function $F \approx 0.001(T/T_K)^2$ as a function U . (b) The increase of the double occupancy relative to its value at the minimum, normalized to the total increase, $\frac{D(T) - D(T_{\min})}{D(0) - D(T_{\min})}$ (T_{\min} is the temperature of the minimum).

Kondo fixed point at $T = 0$. The Kondo scale, estimated from the onset of this scaling behavior via $F(T_K) \stackrel{!}{=} 0.001$, exhibits the expected exponential decrease as a function of U (see upper left inset).

This unusual behavior must be interpreted in the following way. For higher T , as U is increased, charge fluctuations are strongly suppressed by the Coulomb repulsion and are frozen out as the system approaches its local-moment fixed point. This happens on a scale Γ , explaining why $D(T)$ flattens on that temperature scale for all U . At very low temperatures, the system tends to form a Kondo singlet due to spin fluctuations, which are accompanied by virtual charge fluctuations, thereby again enhancing $D(T)$. (Note that the absolute value of this contribution

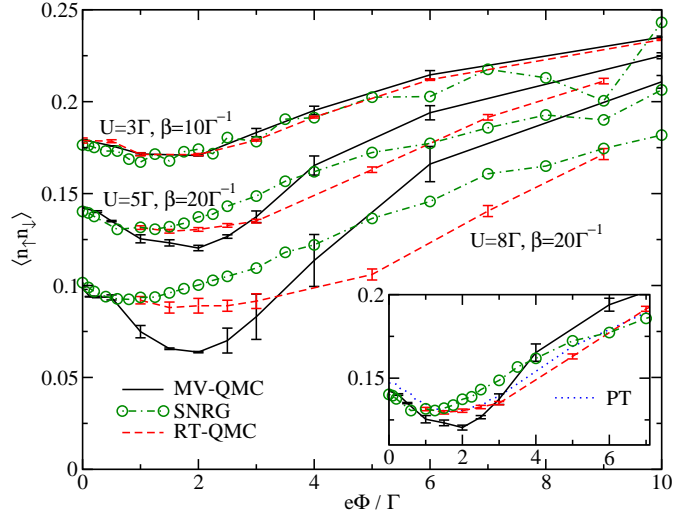


Fig. 3: (color online) Double occupancy as a function of the bias voltage for a broad range of the bias voltage. The inset shows the double occupancy for $U = 5\Gamma$, comparing to second-order perturbation theory (PT). At the present stage of development, significant mutual discrepancies are observed between all computational methods in the intermediate voltage range.

to $D(T)$ is of course again strongly suppressed with increasing U .) This increase produced by Kondo correlations should therefore occur at temperatures on the order of T_K . However, the enhancement of $D(T)$ already set in for temperatures slightly below $\Gamma \gg T_K$ which is observable in the lower right inset of Fig. 2(a) and Fig. 2(b). This is due to the typical logarithmic tails [33] ubiquitous in Kondo systems as visible in Fig. 2(b).

In Fig. 3 we provide non-equilibrium double occupancy data as a function of the bias voltage as obtained from the three approaches discussed above. The overall functional forms look quite similar to the equilibrium curves of Fig. 2. For large bias voltages all methods approach the non-interacting limit $\langle n_{\uparrow} n_{\downarrow} \rangle \xrightarrow{\Phi \rightarrow \infty} \langle n_{\uparrow} \rangle \langle n_{\downarrow} \rangle = 1/4$ and for zero bias voltage $\Phi = 0$ they all reproduce the equilibrium value. (There are no RT-QMC data available for very small voltages, but it seems that the available data extrapolate to the SNRG and MV-QMC result.) At intermediate voltages, all methods produce a minimum. For the weakest interaction, $U = 3\Gamma$, all curves agree quantitatively. However, for larger U , the approaches differ both in the position and in the depth of this minimum.

With increasing U , the MV-QMC approach exhibits the most pronounced minimum, whose position slightly moves to larger voltages. The RT-QMC results show a more shallow minimum, with a position roughly in agreement with MV-QMC. In contrast, the depth of the minimum in the SNRG results does not deepen significantly with U , while the position even appears to move slightly towards smaller voltages.

In Ref. [18] it was shown that low order perturbation

theory results for the current are accurate up to $U/\Gamma \approx 4$, with small deviations in the intermediate voltage regime for $U/\Gamma = 6$. At larger interactions, the perturbation theory result becomes incompatible with RT-QMC in the intermediate bias regime $1 \lesssim V/\Gamma \lesssim 5$ [18]. This is consistent with the findings of this study as shown in the inset of Fig. 3, where the RT-QMC results for U/Γ are close to the prediction from second-order perturbation theory.

The origin of the discrepancies in the nonequilibrium double occupancy for intermediate and large U is unclear. If we assume that SNRG captures the correct position of the minimum in $D(\Phi)$, this would support the notion that a finite bias voltage can act similarly to an increase in temperature. The primary effect of both is to induce larger fluctuations, and therefore the behavior of the double occupancy as a function of temperature and bias voltage is qualitatively the same. Consequently, the position of the minimum does not move significantly with bias voltage and temperature.

On the other hand, the MV-QMC and RT-QMC results suggest that voltage and temperature act in a fundamentally different way on the double occupancy. The shift of the minimum position to larger voltages with increasing U may be a genuine non-equilibrium effect, whose physical mechanism however remains to be clarified.

Magnetic susceptibility. In Fig. 4, we present a comparison of the SNRG and MV-QMC non-equilibrium data for the magnetic susceptibility as a function of the bias voltage for three magnetic fields $B < T_K$. The linear slope of the magnetization curves in a small, but finite magnetic field B , $\chi \sim \frac{\langle n_\uparrow \rangle - \langle n_\downarrow \rangle}{B}$, is taken as an estimate for the susceptibility. Note that the computational effort for the MV-QMC calculations is kept constant throughout the considered parameter range, leading to a doubling of the relative statistical error as the magnetic field is decreased by a factor of two.

The magnetic susceptibility clearly exhibits a signature of the equilibrium Kondo scale, which is in contrast to the double occupancy. The susceptibility drops strongly when the voltage reaches the order of T_K indicating the destruction of the Kondo correlations due to the voltage induced fluctuations. As a function of temperature, this is a well-known fact in equilibrium [7], and can also be shown to hold for non-equilibrium systems, for example, using a simple scaling analysis of simulation data within the Matsubara-voltage formalism [27].

MV-QMC and SNRG agree reasonably well in the low-voltage regime. In both methods well-understood numerical issues lead to a discrepancy with the equilibrium value of the magnetization at $\Phi = 0$. In MV-QMC, this is due to a systematic bias in the MaxEnt estimator and the growth in statistical error at low fields [27]. Within SNRG, the main source of inaccuracies is the truncation of the basis states due to the limited computer memory. Keeping the number of states fixed, this truncation becomes more severe in cases where many states become close in energy,

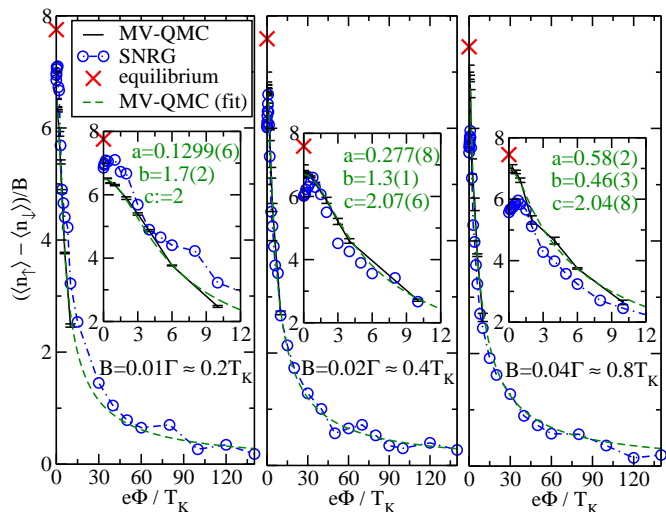


Fig. 4: (Color online) Magnetic susceptibility as a function of the bias voltage (in units of the Kondo temperature) obtained from MV-QMC and SNRG for $U = 8\Gamma$, $\beta = 40\Gamma^{-1}$ at different values of the magnetic field. Within MV-QMC the computational effort is chosen to be identical for each of the curves which renders $B = 0.01\Gamma$ the least and $B = 0.04\Gamma$ the most accurate. The equilibrium limit is shown as the red cross on the $\Phi = 0$ axis. The green dashed line shows a weighted least-square fit of the MV-QMC data to Eq. (5). We used the Haldane estimate of the equilibrium Kondo temperature $T_K \approx \frac{1}{20}\Gamma$. The insets show close-ups of the low voltage region, as well as parameters of the fit to Eq. 5.

which is the case when the voltage, the Kondo scale and the magnetic field are of the same order. A similar behavior of few-states SNRG can be observed for the equilibrium temperature dependence of $m(T)$ (not shown) which can, however, be overcome computationally much more easily than in the non-equilibrium situation.

While the sign problem in quantum Monte-Carlo prevents a direct computation of MV-QMC values at higher voltages, this range is accessible with SNRG. In Ref. [27] we noted that the Matsubara-voltage magnetization data can be described by the expression

$$\frac{m(\tilde{\Phi})}{B} \approx \frac{a}{B} \cdot \frac{1}{\frac{\tilde{\Phi}^2}{\sqrt{b^2 + \tilde{\Phi}^2}} + c}, \quad (5)$$

where $\tilde{\Phi} = \Phi/(\pi T_K)$. The additional square-root in the denominator of Eq. (5) leads to larger tails in the high-voltage regime of the susceptibility when compared to a fit with a pure Lorentz-like function, $\sim \frac{1}{c + \tilde{\Phi}^2}$. This could be interpreted as a precursor of logarithmic tails expected in the Kondo regime [33].

We used this function to fit the low-voltage MV-QMC data in Fig. 4. The first thing to note is that the low-voltage fit results in an excellent description of the SNRG data at high voltages, too. For $B = 0.01\Gamma$, where the MV-QMC data have the largest error, a fit with all three parameters in Eq. 5 became very bad. However, for larger

B with higher quality data, we observe that the parameter $c \approx 2$. Constraining this parameter to $c = 2$ for $B = 0.01\Gamma$ again results in an excellent fit here, too, including the high-voltage data from SNRG. Further analyzing the field dependence of the parameters a and b , we find a surprisingly simple behavior, viz $a \approx 0.75 \cdot B/T_K$ and $b \approx 2(1 - B/T_K)$. We therefore suggest as an approximate, but very accurate formula for the behavior of the local susceptibility at low temperatures and fields $T, B \lesssim T_K$

$$\chi(T, B, \Phi) \approx \frac{\chi(T, B, 0)}{\frac{\Phi^2/4}{\sqrt{(1-B/T_K)^2 + \Phi^2/4}} + 1}. \quad (6)$$

Summary. — In the present paper we have provided a comparison of three state-of-the-art computational methods for two local observables on a quantum dot in a stationary nonequilibrium state, namely the double occupancy and the magnetization. For the double occupancy, which only indirectly exhibits the Kondo temperature as a relevant energy scale, we have found substantial disagreement between all three methods, whose origin is unclear. However, a qualitative agreement between RT-QMC and MV-QMC is found, and for the interaction parameters considered, the RT-QMC gives results in close agreement with second-order perturbation theory.

With regard to the magnetization, we compared MV-QMC and SNRG data within the Kondo regime. In contrast to the double occupancy, we found good agreement between the two methods. This finding is remarkable, because in these calculations, the physics is clearly controlled by the non-equilibrium Kondo effect.

* * *

We thank K. Schönhammer, M. Jarrell, and A. Schiller for useful discussions. This work was supported by the Deutsche Forschungsgemeinschaft under Grant No. AN 275/6-2, FP7/ERC starting grant No. 278023, and the NSF with Grant No. DMR-0907150. We would like to acknowledge computer support from the HLRN, the Goe-Grid initiative, the GWDG, and the NIC, Forschungszentrum Jülich, under Project No. HHB000. Parts of the implementation are based on the ALPS 1.3 library [34].

REFERENCES

- [1] M. A. Kastner, *Rev. Mod. Phys.*, **64**, 849, (1992).
- [2] A.D. Yoffe, *Adv. Phys.* **50**, 1 (2001).
- [3] D. Goldhaber-Gordon, H. Shtrikman, D. Mahalu, D. Abusch-Magder, U. Meirav, and M. Kastner, *Nature* **391**, 156 (1998).
- [4] M. Pustilnik and L. Glazman, *J. Phys.: Cond. Mat.* **16**, R513 (2004).
- [5] S. M. Cronenwett, T. H. Oosterkamp, L. P. Kouwenhoven, *Science* **281**, 540 (1998).
- [6] R.M. Potok, I.G. Rau, H. Shtrikman, Y. Oreg and D. Goldhaber-Gordon, *Nature* **446**, 167 (2007).
- [7] A. C. Hewson, *The Kondo Problem to Heavy Fermions*, Cambridge University Press (1997).
- [8] N. Andrei, K. Furuya and J. H. Lowenstein, *Rev. Mod. Phys.*, **55**, 331 (1983).
- [9] K.G. Wilson, *Rev. Mod. Phys.* **47**, 773 (1975).
- [10] S. Hershfield, J.H. Davies, and J.W. Wilkins, *Phys. Rev. B* **46**, 7046 (1992).
- [11] Y. Meir, N.S. Wingreen, and P.A. Lee, *Phys. Rev. Lett.* **70**, 2601 (1993).
- [12] T. Fujii and K. Ueda, *Phys. Rev. B* **68**, 155310 (2003).
- [13] J. König et al., *Phys. Rev. B* **54**, 16820 (1996); H. Schoeller and J. König, *Phys. Rev. Lett.* **84**, 3686 (2000); S.G. Jakobs, V. Meden, and H. Schoeller, *Phys. Rev. Lett.* **99**, 150603 (2007); M. Pletyukhov and H. Schoeller, *Phys. Rev. Lett.* **108**, 260601 (2012).
- [14] A. Rosch, J. Paaske, J. Kroha, and P. Wölfle, *Phys. Rev. Lett.* **90**, 076804 (2003); *J. Phys. Soc. Jp.* **74**, 118 (2005).
- [15] R. Gezzi, T. Pruschke, and V. Meden, *Phys. Rev. B* **75**, 045324 (2007).
- [16] S. Weiss, J. Eckel, M. Thorwart, and R. Egger, *Phys. Rev. B* **77**, 195316 (2008).
- [17] P. Werner, T. Oka, and A.J. Millis, *Phys. Rev. B* **79**, 035320 (2009).
- [18] P. Werner, T. Oka, M. Eckstein, and A.J. Millis, *Phys. Rev. B* **81**, 035108 (2010).
- [19] F.B. Anders, *Phys. Rev. Lett.* **101**, 066804 (2008).
- [20] E. Boulat, H. Saleur, and P. Schmitteckert, *Phys. Rev. Lett.* **101**, 140601 (2008); F. Heidrich-Meisner, G.B. Martins, C.A. Buesser, K.A. Al-Hassanieh, A.E. Feiguin, G. Chiappe, E.V. Anda, and E. Dagotto, *Eur. Phys. J. B* **67**, 527 (2009).
- [21] D. Segal, A. Millis, D. R. Reichman, *Phys. Rev. B* **82**, 205323 (2010)
- [22] G. Cohen, E. Gull, D. R. Reichman, A. J. Millis, E. Rabani, arXiv:1212.0546
- [23] J. E. Han and R. J. Heary, *Phys. Rev. Lett.* **99**, 236808 (2007).
- [24] E. Gull, A. Millis, A. Lichtenstein, A. Rubtsov, M. Troyer, and P. Werner, *Rev. Mod. Phys.* **83**, 349 (2011).
- [25] A. Dirks, Ph. Werner, M. Jarrell, and Th. Pruschke, *Phys. Rev. E* **82**, 26701 (2010)
- [26] M. Jarrell and J.E. Gubernatis, *Phys. Rep.* **269**, 133 (1996).
- [27] J. E. Han, A. Dirks, and Th. Pruschke, *Phys. Rev. B* **86**, 155130 (2012)
- [28] A. Dirks, J. E. Han, M. Jarrell, and Th. Pruschke, arXiv:1205.1817
- [29] S. Schmitt and F.B. Anders, *Phys. Rev. B*, **81**, 165106 (2010).
- [30] S. Schmitt and F.B. Anders, *Phys. Rev. Lett.* **107**, 056801 (2011)
- [31] F.B. Anders and A. Schiller, *Phys. Rev. Lett.* **95**, 196801 (2005).
- [32] F.B. Anders and A. Schiller, *Phys. Rev. B* **74**, 245113 (2006).
- [33] R. Bulla, M.T. Glossop, D.E. Logan, and T. Pruschke, *J. Phys. Condens. Matter* **12**, 4899 (2000). N.L. Dickens and D.E. Logan, *J. Phys. Condens. Matter* **13**, 4505 (2001). A. Rosch, J. Paaske, J. Kroha, and P. Wölfle, *Phys. Rev. Lett.* **90**, 076804 (2003).
- [34] A.F. Albuquerque et al., *Journal of Magnetism and Magnetic Materials* **310** (2), 1187 (2007).